Theoretical Assessment of Corannulene-Based Aggregates as High-Performance Nonlinear Optical Materials

MS Thesis

by

Sobia Waheed

CIIT/SP22-R06-024/LHR

COMSATS University Islamabad

Lahore-Pakistan

Fall 2023

Theoretical Assessment of Corannulene-Based Aggregates as High-Performance Nonlinear Optical Materials

A thesis submitted to
COMSATS University Islamabad

In partial fulfillment
of the requirements for the degree of

Master of Science
in
Chemistry
by

Sobia Waheed
CIIT/SP22-R06-024/LHR

Department of Chemistry
Faculty of Sciences

COMSATS University Islamabad
Lahore-Pakistan
Fall 2023

Theoretical Assessment of Corannulene-Based Aggregates as High-Performance Nonlinear Optical Materials

This thesis is submitted to the Department of Chemistry in partial fulfilment of the requirements for the award of the degree of Master of Science in Chemistry.

Name	Registration number
Sobia Waheed	CIIT/SP22-R06-024/LHR

Supervisory Committee

Supervisor
Dr. Mazhar Amjad Gilani
Associate Professor
Department of Chemistry
COMSATS University Islamabad (CUI)
Lahore campus

Member
Dr. Muhammad Shahid Nazir
Associate Professor
Department of Chemistry
COMSATS University Islamabad (CUI)
Lahore campus

Member
Dr. Sobia Tabassum
Associate Professor
Interdisciplinary Research Centre in Biomedical Materials (IRCBM)
COMSATS University Islamabad (CUI)
Lahore campus

Certificate of Approval

This thesis titled

Theoretical Assessment of Corannulene-Based Aggregates as High-Performance Nonlinear Optical Materials

By

Sobia Waheed
CUI/SP22-R06-024/LHR

has been approved

for the Degree of Master of Science in Chemistry
at COMSATS University Islamabad, Lahore Campus

External Examiner: _____

Dr. Riaz Hussain (Assistant Professor)
Department of Chemistry
University of Okara,
Okara, Punjab, Pakistan

Supervisor: _____

Dr. Mazhar Amjad Gilani (Associate Professor)
Department of Chemistry
CUI, Lahore campus

Head of Department: _____

Prof. Dr. Zulfiqar Ali
Department of Chemistry
CUI, Lahore campus

Author's Declaration

I Sobia Waheed, CIIT/SP22-R06-024/LHR, hereby declare that I have produced the work presented in this thesis, during the scheduled period of study. I also declare that I have not taken any material from any source except referred to wherever due to that amount of plagiarism is within an acceptable range. If a violation of HEC rules on research has occurred in this thesis, I shall be liable to punishable action under the plagiarism rules of HEC.

Date: _____

Sobia Waheed

CIIT/SP22-R06-024/LHR

Certificate

It is certified that Sobia Waheed, CIIT/SP22-R06-024/LHR, has carried out all the work related to this thesis under my supervision at the Department of Chemistry, COMSATS University Islamabad, Lahore campus and the work fulfils the requirements for the award of the degree of MS in Chemistry.

Date: _____

Supervisor

_____

Dr. Mazhar Amjad Gilani

Associate Professor

Department of Chemistry

COMSATS University Islamabad

Lahore Campus

Dedication

To My Beloved Parents

Acknowledgments

All praises are for **Allah** who is the **Creator** of the Universe. He is the most beneficent and most **merciful.** All gratitude and prayers belong to **Him** and peace be upon **Hazrat Muhammad (S.A.W)** His last messenger and servant. I am deeply grateful to **Allah Almighty** for giving me the strength to apprehend my work and for enabling me to stand strong and optimistic in ups and downs during the whole time.

First and foremost, I have a great inspiration for my supervisor, Dr. Mazhar Amjad Gilani (Associate professor), CUI Lahore Campus, Pakistan, whose thoughtful suggestions and guidance as well as very compassionate and welcoming attitude kept me high-spirited throughout my research work. He has been supportive since the days I began working on the project in his lab.

I would also like to express my gratitude to the Head of Department Prof. Dr. Zulfiqar Ali and my teachers at CUI Lahore, including Dr. Shahid Nazir, Dr. Sadaf -ul- Hassan, Dr. Javed Iqbal, Dr. Sara Riaz and Dr. Lubna and all other respected faculty. Their pedagogy and keenness for their respective subjects made a strong impression on me and I have always carried great memories of their classes with me. I also express my appreciation for the rest of staff for their support and help towards my graduation.

Profound gratitude to my seniors, Ms. Rehana Bano (PhD scholar), Ms. Palwasha Khan (PhD scholar), Ali Hussain, Khalida Khalil, Dua Fatima, Mawra Nasir, M. Ahtisham, M. Adeel and other lab mates for their continuous guidance and support.

Finally, yet importantly my heartfelt gratitude to my beloved parents and my siblings for their prayers, everlasting love and support.

Sobia Waheed

CIIT/SP22-R06-024/LHR

Abstract

Theoretical Assessment of Corannulene-Based Aggregates as High-Performance Nonlinear Optical Materials

BY

Sobia Waheed

The growing use of nonlinear optical (NLO) materials in various fields has generated interest in designing innovative smart NLO materials. This study focuses on enhancing the nonlinear optical response through doping of alkali metals on the corannulene ($C_{20}H_{10}$) dimer through Density Functional Theory (DFT) calculations.-The interaction energies calculated computationally confirm the stability of the newly designed alkali metal-doped cncx dimers. Alkali metal doping, particularly with Li, Na, and K, leads to a significant reduction in the $E_{(H–L)}$ gap, and the lowest energy gap of 3.17 *eV* is observed in K-doped cncx dimer. The TD-DFT study shows that these alkali metal doped complexes have λ_{max} in the visible regions(568-576nm). Total density of states (TDOS) spectra support the involvement of dimer in forming new Highest Occupied Molecular Orbital (HOMO). Natural Bond Orbital (NBO) analysis validates substantial charge transfer from alkali metals to dimer, with the highest charge transfer (0.938 $|e|$) observed in the K@cncx complex. Doping with alkali metals enhances the first hyperpolarizability, and Li@cncx exhibits the highest value (9.3×10^4 *au*). The study also determines frequency-dependent Second Harmonic Generation (SHG), Electric-Optical Pockels Effect (EOPE), electro-optic dc-Kerr effect (EOKE). The value of 3.4×10^4 *au* is observed for SHG, while for EOPE the value is 4.6×10^5 *au*. A significantly enhanced EOKE value (1.0×10^{10} *au*) is shown by Na@cncx. Additionally, these structures exhibit a high nonlinear quadratic refractive index (a maximum value of $9.9\times10^{-18} cm^2 W^{-1}$). In conclusion, the study provides guidelines for computationally designing efficient and thermodynamically stable complexes for optical and optoelectronic technologies.

Table of Contents

List of Figures

List of Tables

List of Abbreviations

IR	Infrared
UV	Ultraviolet
NLO	Nonlinear Optical
DFT	Density Functional Theory
TDOS	Total Density of States
HOMO	Highest Occupied Molecular Orbital
NBO	Natural Bond Orbital
SHG	Second Harmonic Generation
EOPE	Electric-Optical Pockels Effect
EOKE	Electro-Optic dc-Kerr Effect
MOFs	Metal-Organic frameworks
PAH	Polycyclic Aromatic Hydrocarbon
PDOS	Partial Density of State
QTAIM	Quantum Theory of Atoms in Molecules
BCPs	Bond Critical Points
IRI	Interaction Region Indicator
FMO	Frontier Molecular Orbitals
ΔE	Excitation Energies

E_{int} Interaction Energies

E_g Energy Gap

cxcx Convex-Convex

cncn Concave-Concave

cncx Concave-Convex

AM@cncx Alkali metal doped dimer

Chapter 1
Introduction

1.1 Origin of Nonlinear Phenomena

Theoretical basis for nonlinear phenomena was established in the 1930s. With the invention of lasers in the 1960s, nonlinear effects were first observed. Laser lights have high intensities, so they are very important to produce the nonlinear response of material.

1.2 Optics

The field of optics explores how electromagnetic waves interact with matter, commonly dealing with infrared (IR), ultraviolet (UV), and visible light. when light interact with matter then the material respond differently. Interactions between matter and light can be either linear or nonlinear. The polarization field is directly linked to the incident electric field if the intensity of light is low.

1.2.1 Linear Optics

Linear optics, being independent of light intensity, results in no alteration of light properties, as presented in **Figure 1.1**. Even though light may be redirected away from the material, its frequency remains unchanged. When employing a linear approach, an insufficient external field is no longer a factor to consider.

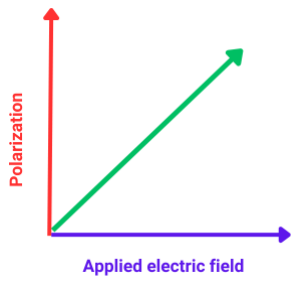

Figure 1.1: Illustration of linear optical response

1.2.2 Nonlinear optics

When a material encounters a strong laser beam with an electromagnetic field, it produces electromagnetic radiations with different phases, frequencies, and amplitudes as it moves, causing NLO phenomena as shown in **Figure 1.2**. Under the influence of such high-intensity light, the optical traits of the medium can be altered, introducing processes not observed in materials that respond linearly to optical forces. These phenomena can result in alterations to the spectral, spatial, or polarization characteristics of the light beam and can even lead to the creation of entirely new frequency components.

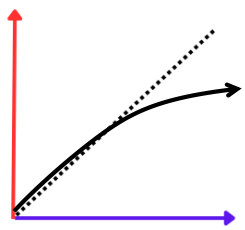

Figure 1.2: Nonlinear optical effect

The interaction between laser beam and material results in the generation of electric polarization. This, in turn, gives rise to a variety of unique and captivating optically

nonlinear characteristics, facilitating the potential for achieving phase matching or index matching. Nonlinear optics include the following effects such as second harmonic generation, parametric effects, sum and difference frequency mixing, frequency up and down conversion, parametric amplification and oscillation, four-wave mixing phenomena, Raman effect, Brillouin effect, and the Optical Kerr effect. The propagation of light in nonlinear optical media is accompanied by self-phase modulation. In Second Harmonic Generation (SHG) when the light falls on the materials then there will be the transformation of light signals, resulting in an output wave with a frequency exactly twice that of the initial wave [1] as presented in **Figure 1.3**.

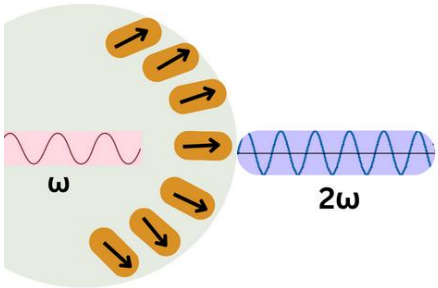

Figure 1.3: Second harmonic generation

1.2.3 Linear and Nonlinear polarization

When electric field of light interact with the matter then the material' polarization takes place. This polarity in response to the external field leads to a broad spectrum of outputs, which may involve oscillations at comparable or distinct frequencies.

1.4 Applications of Nonlinear Optics

NLO materials are such materials that has wide applications in many fields like electro-optic and photonic devices, optical switching, optical limiting, optical communications, signal processing, sensing and so on.

1.5 Nonlinear Optical Materials

1.5.1 Inorganic NLO materials

Certain well-established oxide nonlinear optical (NLO) materials, including borates like β-BaB_2O_4 (BBO) [27] and LiB_3O_5 (LBO) [28], as well as phosphates such as KH_2PO_4 (KDP) [29] and $KTiOPO_4$ (KTP) [30], are capable of meeting practical needs in the UV and vis-NIR spectral ranges, respectively. Although inorganic materials exhibit a good NLO response, their application is hindered by a low laser damage threshold [31].

1.5.2 Organic NLO materials

Organic materials have garnered significant attention as viable alternatives to their inorganic counterparts due to their enhanced linearity, higher optical susceptibilities [19], faster response times, and greater resistance to damage [32]. When compared to inorganic materials, organic counterparts offer several distinct advantages. They stand out for their rapid and substantial nonlinear response across a wide frequency spectrum. This, coupled with their inherent synthetic adaptability and high optical damage threshold, imparts remarkable properties to these materials [1].

The exceptional optoelectronic characteristics of organic single crystals stem from the presence of delocalized electrons within organic molecules, specifically in conjugated electron systems. These systems manifest various photoresponses, including photoconductive, photovoltaic, and photocatalytic behaviours.

1.6 Buckybowls

In 1985, Kroto and his colleagues pioneered the discovery of fullerene, a novel allotropic form of carbon [33]. Fullerenes are carbon structures characterized by sp2 hybridization, forming polyhedral cages with resonating π electrons [34, 35]. The versatile properties of fullerenes have made them a focal point of research in diverse fields, notably in biomedical [36] , information technology [37] , optoelectronics [38].

Utilizing fullerenes in organic electronics, especially in areas like photovoltaic applications and molecular wires, not only advances research but also underscores the viability of these carbon allotropes for tangible, practical applications [39].

Buckyballs, such as spherical fullerenes like C_{60}, are stable carbon clusters featuring 20 hexagons and 12 pentagons, giving them the appearance of a soccer ball [40]. Buckybowls form intermolecular complexes [41-46]. Given their remarkable and superior qualities, these compounds stand out as excellent candidates for applications in molecular electronics, material sciences, and optoelectronics [47].

Buckyball has numerous uses in a variety of fields [48, 49]. The structure of these buckybowls can be manipulated by changing size, shape and edge geometry [50].

Corannulene ($C_{20}H_{10}$) and its derivatives, known as buckybowls, have been extensively studied and reviewed for their potential applications in different fields. Barth and Lawton were the first to successfully synthesize corannulene in 1966 [51]. X-ray investigation confirmed that the molecule is structured in the shape of a bowl with a depth of 0.87 Å [52]. Corannulene [47, 53-64] is frequently characterized as the smallest fragment of fullerene C_{60} that maintains a curved molecular structure. It has bowl like structure having concave side and convex side.Its structure is composed of five benzene rings fused with central pentane ring [65]. Carbon atoms of the corannulene provide distinct π-electron densities to the structure [66].

1.7 Aggregates

The transfer of electrons within aggregates is influenced by linker compounds, actively participating in the delocalization of electrons across the structure. Structures formed by noncentrosymmetric organic molecules through repetitive π-π stacking demonstrate nonlinear optical (NLO) traits [67]. Aggregates not only influence the emissions but also have wide range of applications in many fields [68].

The dimer of corannulene exist in the various π–π stackings like concave-convex, convex-convex, concave-concave. Most interactions in π–π stacking involve molecules connecting through π–π interactions and these interactions are involved in

enhancing the NLO response [69]. Both inter- and intramolecular interactions within corannulene exert a substantial influence on its physical and chemical traits.

1.8 Leveraging of π–π interaction of Buckybowls in NLO Material Engineering

The substantial π–π interaction significantly boosts charge carrier mobility, suggesting a highly advantageous scenario [70]. The unique curved surface, boasting π-electrons and taking on a bowl-shaped, geodesic polycyclic aromatic hydrocarbon (PAH) structure [71, 72]. π–π interactions are important in the formation of supramolecular assemblies. Corannulene molecules are involved in the formation of supramolecular assemblies such as corannulene -fullerene assemblies exist in gas phase [73]. Due to strong π–π interactions different energetically stable configurations are present. The concave–convex alternative is considered the most energetically favourable arrangement as it maximizes the van der Waals contacts between the dimer. Significant π–π interactions exist among the buckybowls. Different interactions between the convex face of buckybowls and the concave surface of corannulene were confirmed by density functional theory [74]. A significant portion of these interactions include dispersion forces, which play a vital role in supramolecular assemblies.

1.9 Research Gap

A high nonlinear optical response is the prerequisite for a material to be employed in optoelectronics. Alkali metal doped aggregates of corannulene have strong π–π interactions that result in the high transition dipole moment of these aggregates. Due to the high transition dipole moment these aggregates are expected to show high nonlinear optical response and may act as stable NLO materials.

1.10 Current investigation

Corannulene concave convex dimer doped with Li, Na, and K metals to examine its NLO characteristics.

1.11 Objectives

1. To investigate the geometrical parameters of corannulene-based aggregates

2. To explore the charge transfer behaviour of designed aggregates

3. To explore the intermolecular interactions of aggregates

4. To investigate the polarizability and hyperpolarizability of designed aggregates

Chapter 2
Literature Review

The phenomena of nonlinear optics came into light in 1961. Peter and his team fall red light on the quartz and in turn near-UV light came out 1961, [75]. Within short time other scientist conducted experiments and concluded that there is influence of electric field of light on the frequency modulation of light signals [76]. Franken et al, discovered the nonlinear optical effect such as second harmonic generation [76]. The aggregation of corannulene was reported in 1992, revealing the formation of a sandwich structure with four lithium ions [77].

Calix [4]arene molecule has hyperpolarizability that is significantly enhanced by the presence of alkali metal atoms. Among them, the Li@calix[4]arene complex exhibits the greatest increase in nonlinear optical (NLO) response [78, 79]

These concave–convex π-faces, with their asymmetrical polarization, are especially appealing for supramolecular assembly. Corannulene has concave and convex faces [80]. The NLO response of Li@calix[4]pyrrole and Li+(calix[4]pyrrole) was investigated by Chen et al. A hyperpolarizability value between 7.33×10^3 au and 2.45×10^4 au was computed [17].

In 1964, Franken and his team observed second-harmonic generation (SHG) for the first time in an organic material [81]. A theoretical investigation in a different study explored the influence of doping revealing a considerable increase in the first hyperpolarizabilities.

Alkali metal doped $Al_{12}N_{12}$ nanocage was studied through ab initio calculations. Through these calculations it was revealed that due to the doping a significant hyperpolarizability upto 8.89×10^5 au was observed [82].

Sohail *et al*, concluded that dimers are thermodynamically stable. Buckybowls exist in supramolecular assemblies and dimers. In the buckybowls there was maximum charge observed due to the formation of aggregates [83].The concave and convex faces fit together, forming a close π–π dimer [84].Dimers exhibit the high thermal stability [85]. Liu et al, revealed that corannulene exist in the form of stacking. These stacking had significant hyperpolarizability [86].

The polarizability and first hyperpolarizability of Phosphides or nitrides nano-cages are dramatically enhanced by the alkali metal atoms [87].In the theoretical study of gold-germanium bimetallic clusters it was explored that doping has influence on the NLO properties of material [88].

The doping approach is the main factor influencing the potassium-doped $B_{12}P_{12}$ nanocage's hyperpolarizability value of 7.9×10^5 *au* [89]. Alkali metal adsorbed graphene, graphyne and graphdiyne has greatest increase in NLO response [90]**.**The nonlinear optical effect was initially described and predicted by Maria Goeppert Mayer in 1931, but it remained a theoretical concept until thirty years later when Kaiser and Garrett observed the nonlinear effect in crystals. The invention of the Kerr lens mode-locked femtosecond laser in 1991 played a pivotal role in advancing this field [91].

In a study carried out by Ali Ahmadi Peyghan *et al*., it was revealed that the doping has impact in changing the electronic properties of the system Additionally, alkali metal doping modifies the material's conductive characteristics. There was a shift in the HOMO–LUMO energy gap from 3.77 *eV* to 1.11–1.95 *eV* [92].

The most thermodynamically stable compound is the Li-doped C_{24} complex, with an interaction energy of -190.78 *kcal/mol*. The initial hyperpolarizability is greatly increased by doping with alkali metal atoms (Li, Na, and K), with Na_3C_{24} showing the highest value of 2.74×10^5 au among all C_{24} complexes [93].

Different studies show that the doping causes thermodynamic stability, increase in the hyperpolarizability value. In another study, Na_3C_{24} exhibit the hyperpolarizability up to 2.74×10^5 *au* after doping with alkali metals.

The largest value of (910,706.43 *au*) was recorded in K (BC)Ca, which is boosted by the higher transition dipole moment *(Δμ)* [94]. In lithium atom-doped hexalithioborazine ($B_3N_3Li_6$-Li), the dipole moment is measured at 1.608 *D*, indicating charge transfer. Notably, these complexes show a maximum in charge transfer [95].

Muhammad Rashid et al. investigated The Li@BP nanosheet's Isomer II-Li exhibits the maximum binding energy, measured at −26.36 *kcal/mol* [23].

Chapter 3
Computational Methodology

3.1 Geometry Optimization and Frequency Analysis

For calculations and visualizations of geometries Gaussian 16 software and Gauss View 6.1.1, [96] [97]. The geometries were visualized using Gauss View 6.1.1, [96]. *ωB97XD/6-31G+(d,p)* level of theory was used for the optimization of all the complexes. *ωB97XD* is extensively utilized for accurate computations of non-covalent interactions [98]. On the same level of theory, frequency calculations were carried out to validate the true minima.

3.2 Interaction Energies and Other Ground State Properties

Natural bond orbital (NBO) analysis, Interaction energies *(E_{int})* and energy gap were calculated at *ωB97XD/6-31G+(d,p)* to explore the charge transfer, thermodynamic stability of the complexes. The E_{int} for alkali metal-doped cncx complexes was obtained using the following equation:

$$E_{int} = E_{AM@cncx} - (E_{cncx} + E_{AM}) \quad (1)$$

Where, $E_{AM@cncx}$ = Energy of complex

E_{cncx}= Energy of dimer

E_{AM}= Energy of alkali metal

To calculate the energy gap of all the complexes the following euation can be used :

$$E_{(HOMO)-(LUMO)} = E_{LUMO} - E_{LUMO} \quad (2)$$

Where $E_{(HOMO-LUMO)}$ is the energy of band gap

E_{HOMO}=Energy of HOMO

E_{LUMO}= Energy of LUMO

3.3 Density of States Analysis

The total density of state (TDOS) and partial density of state (PDOS) of the metal doped dimer were visualized using Multiwfn software [99].

3.4 Dipole Moment, Excitation Energies, and Absorption Characteristics

By using *ωB97XD/631+G (d, p),* excited-state dipole moment (μ) and excitation energies ΔE

were estimated. The same functional and basis set is used to compute λ_{max} of both cncx and AM@cncx complexes.

3.5 Dipole moment and Polarizability

The dipole moment plays a key role in determining nonlinear optical characteristics. With higher dipole moment values, there is increased charge dispersion, leading to an enhanced nonlinear optical response. The dipole moment and polarizability can be expressed as;

$$\mu_{\circ} = (\mu_x^2 + \mu_y^2 + \mu_z^2)^{1/2} \quad (3)$$

$$\alpha_{\circ} = \frac{1}{3}(\alpha_{xx} + \alpha_{yy} + \alpha_{zz}) \quad (4)$$

3.6 Hyperpolarizability

The CAM-B3LYP/6-31+G(d,p) method was used to calculate the refractive indices *(n2),* static hyperpolarizability *($\beta_{\circ}$),* dynamic hyperpolarizability, and second hyperpolarizability *(γ).*

$$\beta_{\circ} = \left[\beta_x{}^2 + \beta_y{}^2 + \beta_z{}^2 \right]^{1/2} \quad (5)$$

Where,

$$\beta_x = \beta_{xxx}, \beta_{xyy}, \beta_{xzz}$$

$$\beta_y = \beta_{yyy}, \beta_{yzz}, \beta_{yxx}$$

$$\beta_z = \beta_{zzz}, \beta_{zxx}, \beta_{zyy}$$

And the second hyperpolarizability can be defined as:

$$\gamma_{tot} = \sqrt{\gamma_x^2 + \gamma_y^2 + \gamma_z^2} \quad (6)$$

3.7 Frequency Dependent Calculations

The first dynamic hyperpolarizability can be expressed as:

$$\beta_{(\omega)} = (\beta_{\boldsymbol{x}}(\omega)^{\mathbf{2}} + (\beta_{\boldsymbol{y}}(\omega)^{\mathbf{2}} + (\beta_{\boldsymbol{z}}(\omega)^{\mathbf{2}})^{\mathbf{1}/\mathbf{2}} \quad (7)$$

The traditional sum-over-state (SOS) equation was used to calculate quadratic nonlinear refractive indices *(n_2)* and dynamic second hyperpolarizabilities *(γ (ω))* at different wavelengths such as 1340, 1550, 1907 *nm*.

Chapter 4
Results and Discussion

4.1 Geometric and Energetic Analyses

The corannulene concave-convex (cncx) dimer was optimized using the *ωB97XD/6-31G+(d,p)* level of theory. The structure of corannulene comprises one 5-membered ring surrounded by five 6-membered rings. There are distinct C-C bonds namely, rim, flank, spoke and hub as presented in **Figure 4.1.** The calculated bond lengths rim (1.38 Å), flank (1.38 Å), spoke (1.38 Å), and hub (1.41 Å) align well with the bond lengths observed experimentally for the corannulene molecule [100]. The chosen ωB97XD/6-31G+ (d, p) is reliable for the calculation of dimer because of the agreement between theoretical and experimental results.

There are six doping positions on corannulene such as rim (Rr), hub (Rh), spoke (Rs), flank (Rf), centre of 6-membered ring (R6) and centre of 5- membered **ring** (R5) as shown in **Figure 4.1.**

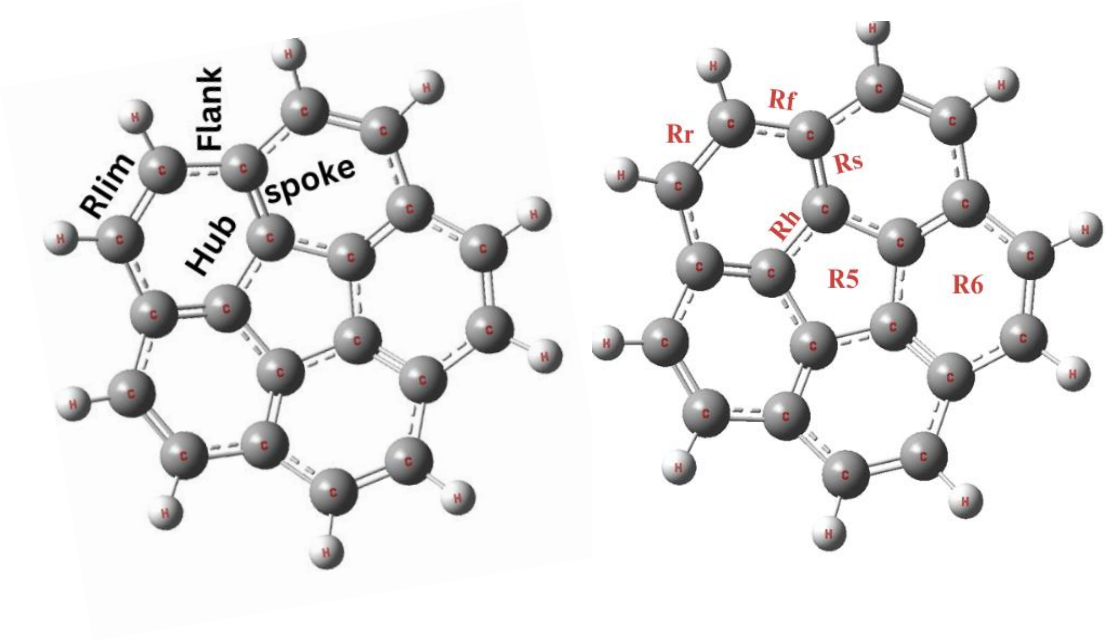

Figure 4.1: Possible doping positions to optimize alkali metals on cncx dimer.

Corannulene displays various stacking models, including concave-concave (cncn), concave-convex (cncx), and convex-convex (cxcx). The most stable among them is the concave-convex(cncx) dimer [101]. In the present study cncx dimer was used for further analysis. Stable complexes are formed when alkali metals are doped on the cncx dimer [102].

Theoretical investigations were conducted on the interaction between alkali metals and dimer, considering all potential positions three geometries were optimized(one for each alkali metal). These complexes (AM@cncx) possess the C1 point group. The optimized shapes of dimer and the alkali metal-doped dimer (AM@cncx) where AM = Li, Na, K) are shown in **Figure 4.2.**

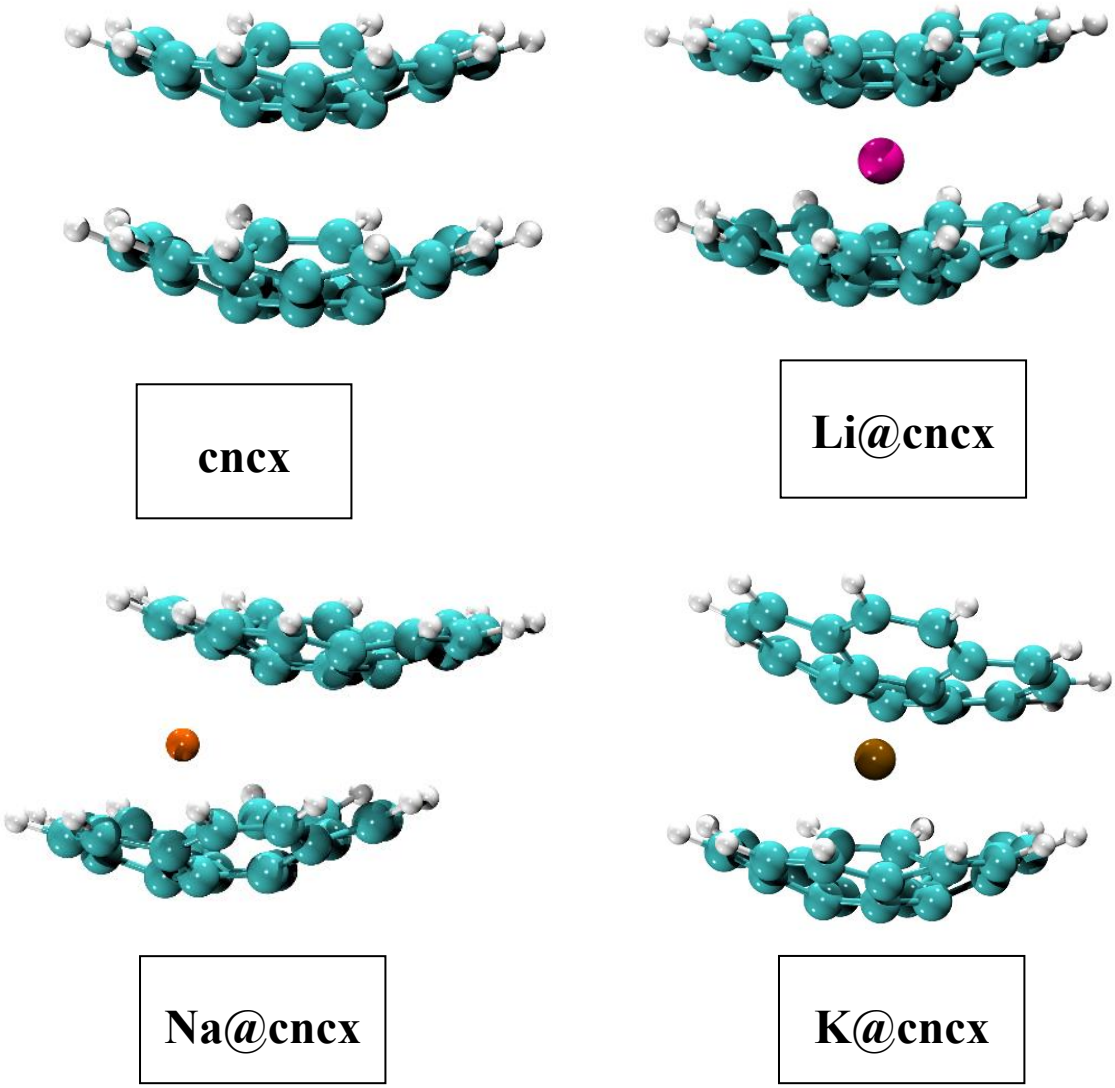

Figure 4.2: The optimized geometries of cncx-dimer and AM@cncx complexes (AM = Li, Na, K)

By calculating interaction distances ($d_{C\text{-}AM}$), we assessed the separation between metals and neighboring carbon atoms in cncx. The interaction distances range from 2.35 *Å* to 3.0 *Å* for AM@cncx.

Table 4-1: Symmetry, Interaction energies (kcal/mol) and Average interaction distances (*Å*), of cncx-dimer and AM@cncx complexes

Complex	**Symmetry**	**E_{int}** *(kcal/mol)*	**d_{AM-C}(*Å*)**
cncx	C1	-20	3.66
Li@cncx	C1	-34.5	2.35
Na@cncx	C1	-23.8	2.61
K@cncx	C1	-22.2	3.0

d_{AM-C}=Distance between interacting metal and carbon atom

With the increase in atomic no, the interaction distance increases. The interaction distance tends to be greater for large size atoms due to significant repulsion caused by extensive electronic cloud. when the atomic size increases the charge is dispersed over a larger sphere and binding interactions weakens [103].This may lead to the increase of the distance between the dimer. Doping corannulene dimers with alkali metals, especially the larger ones, may induce an expansion of the distance between the dimer, owing to a combination of repulsive forces between the alkali metal and potential changes in electrostatic and van der Waals interactions.

The distance 2.35*Å* was observed in Li@cncx with the interaction energy of -34.5 *kcal/mol* with the decrease in distance the interaction energy increases [104].

The theoretical calculations yielded interaction energies of -34.5, -23.8, and -22.2 *kcal/mol* for the AM@cncx complexes.

4.2 Natural bond orbital (NBO) analysis

NBO confirm the amount of charges which is being transferred from alkali metal to dimer. During NBO analysis the negative charges show the charge is being accepted by the species and the positive charge shows the charge is being transferred from that specie. In all the complexes the positive charges are present on the metals and the

negative charges are present on the dimer which shows the transference of electrons from metals to dimer. The corannulene buckybowl is well-known for its ability to accept electrons [45]. NBO charges on the alkali metals ranges from 0.882 to 0.938 |*e*| in all complexes as detailed in **Table 4.2.** The maximum amount charge transfer (0.938 |*e*) is observed in K@cncx complex. These results show that potassium is transferring its maximum electron density to the dimer.

4.3 Electronic Properties

The energies and isodensities of the highest molecular orbitals (HOMO) and lowest unoccupied molecular orbitals (LUMO) were determined. In its original state, corannulene exhibits a substantial energy gap of 7.4 *eV*, imposing limitations on its utility in optoelectronic devices. The energy gap (E_g) is important to conductance, semiconductance, and insulation properties of the complexes [6]. The energies of HOMO and LUMO and energy gap (E_g) are presented in **Table 4.2.**

Table 4-2: NBO charges, Energy gap (Eg), and the energies of HOMO and LUMO of cncx-dimer and AM@cncx complexes

Complexes	**HOMO (eV)**	**LUMO (eV)**	**E_g *(eV)***	**NBO Charges Q_{AM} |e|**
cncx	-7.76	-0.32	7.44	___
Li@cncx	-4.35	-0.67	3.68	0.89
Na@cncx	-4.16	-0.79	3.38	0.88
K@cncx	-4.01	-0.84	3.17	0.94

HOMO-LUMO energy gap (E_g) is less in all the metal complexes. The range of energy gap is from 3.17 to 3.68 *eV*, which is less as compared to the E_g of the dimer, which is 7.44 *eV.* The diffuse electrons of the alkali metals cause a rise in the energy level of HOMO. Among the complexes, K@cncx shows the most substantial reduction in E_g, reaching a minimum of 3.17 *eV.* The percentage reduction of energy gap is 57.52% in K@cncx while Li@cncx exhibits the lowest percentage reduction of Eg (50.67%). In Li@cncx, the E_g is the highest at 3.68 *eV*, followed by Na@cncx at 3.38 *eV*. HOMO -LUMO densities are presented in **Figure 4.3.**

Complexes	HOMO	LUMO
cncx	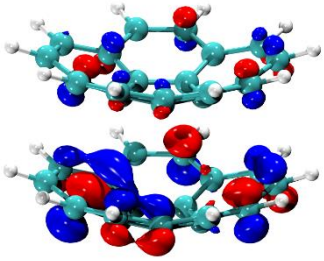	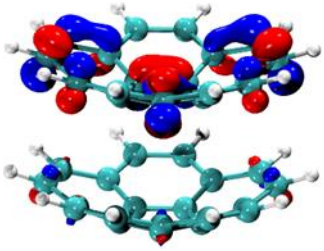
Li@cncx	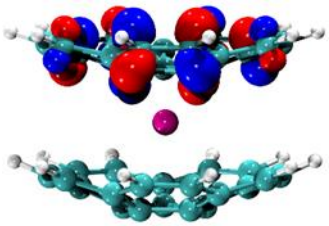	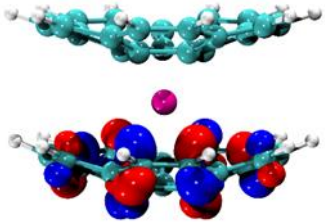
Na@cncx	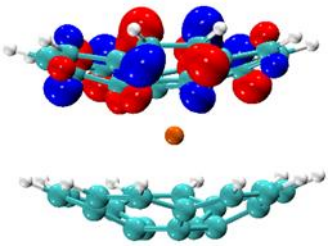	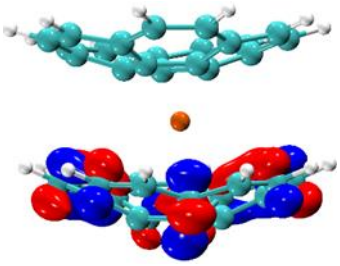
K@cncx	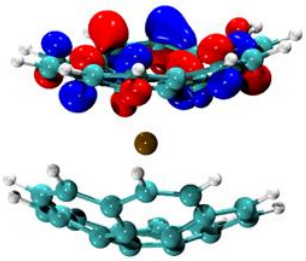	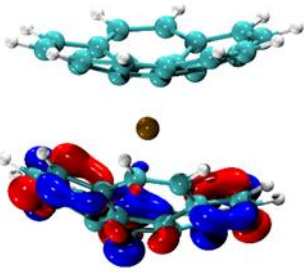

Figure 4.3: Frontier molecular orbitals of dimer and alkali metal doped complexes.

In all the alkali metal-doped dimers, HOMO densities lie on the convex, and LUMO density lies on the concave side of dimer. This indicates that the dimer is involved in the creation of a new HOMO.

4.4 QTAIM analysis

To assess the intermolecular interactions between the dimer, the quantum theory of atoms in molecules (QTAIM) was carried out [105-107]. Different topological parameters are used to identify the bond critical points (BCPs).These parameters are energy density G(r) electronic potential energy density V(r) electron density *(ρ) and* Laplacian of electron density ($\nabla^2\rho$). Strong covalent interactions are indicated by an a -V(r)/G(r) ratio < 0.5, a negative ∇^2 electron density *(ρ)* > 0.1 *au*. when the ρ < 0.1 *au*, the -V(r)/G(r) >0.5 and $\nabla^2\rho$ is positive then the week van der Waals interactions will exist. The equations provided can be used to represent Bond Critical Points (BCPs)

$$H_r = G_r + V_r \quad (1)$$

$$\left(\frac{1}{4}\right)\Delta^2\boldsymbol{\rho}_r = 2G_R + v_r \quad (2)$$

When analyzing the values of different topological parameters for all AM@cncx complexes, it is concluded that weak van der Waals interactions exist between the dimers, as outlined in

Table 4-3: ρ, $\nabla^2\rho$ V(r), -V(r)/G(r) and G(r) parameters at BCPs of cncx-dimer and AM@cncx complexes

(All the values are in *au*)

Complex	**Interaction**	ρ	$\nabla^2\rho$	**G(r)**	**V(r)**	**H(r)**	**G(r)/V(r)**
cncx	C31-C11	0.0059	0.0167	0.0034	-0.0027	0.0007	1.2592
Li@cncx	Li-C32	0.0148	0.0159	0.0159	-0.0121	-0.0037	1.314

	Li-C17	0.0168	0.0925	0.0189	-0.0148	0.0041	1.277
	Li-C12	0.0161	0.0925	0.0187	-0.0143	0.0043	1.3062
	C 49-C9	0.0039	0.0096	0.0020	-0.0017	0.0003	1.1765
	C50-C10	0.0041	0.0099	0.0021	-0.0018	0.0003	1.1667
	C47-C15	0.0073	0.0203	0.0042	-0.0033	0.0008	1.2727
	C35-C16	0.0041	0.0098	0.0021	-0.0018	0.0002	1.1666
	C48-C14	0.0068	0.0197	0.0041	-0.0032	0.0008	1.2812
	C39-C14	0.0069	0.0200	0.0041	-0.0033	0.0008	1.2424
	C36-C19	0.0039	0.0096	0.0020	-0.0017	0.0003	1.1765
	C38-C13	0.0036	0.0203	0.0042	-0.0034	0.0008	1.235
Na@cncx	Na-C43	0.0112	0.0570	0.0117	-0.0093	0.0024	1.2581
	Na-C18	0.0128	0.0634	0.0132	-0.0105	0.0026	1.2571
	Na-C11	0.0130	0.678	0.0138	-0.0108	0.0030	1.2778
	C35-C11	0.0025	0.0064	0.0013	-0.0010	0.0002	1.3
	C38-C14	0.0088	0.0263	0.0054	-0.0042	0.0011	1.2857
	C47-C9	0.0024	0.0062	0.0013	-0.0010	0.0002	1.3
K@cncx	K-C41	0.0095	0.0393	0.0081	-0.0065	0.0016	1.2461

	K-C13	0.0128	0.0525	0.0109	-0.0087	0.0021	1.2529
	K-C2	0.0107	0.0420	0.0087	-0.0070	0.0017	1.2428
	K-C3	0.0107	0.0417	0.0087	-0.0070	0.0017	1.2428
	C60-C7	0.0050	0.0153	0.0030	-0.0022	0.0007	1.3636
	C60-C7	0.0091	0.0295	0.0058	-0.0042	0.0015	1.380

Topological diagrams with BCPs marked in orange for dimer and all AM@cncx complexes are presented in **Figure 4.4.**

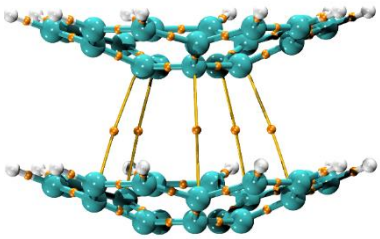

cncx

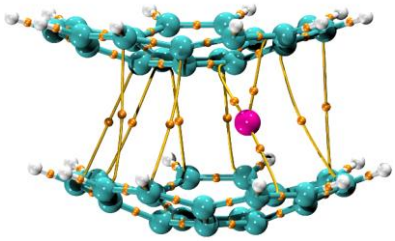

Li@cncx

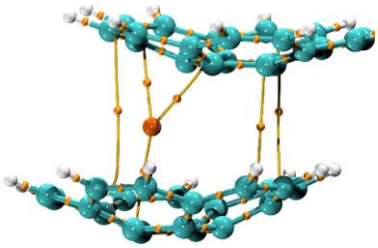

Na@cncx

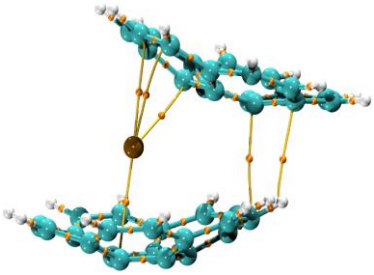

K@cncx

Figure 4.3: Topological diagrams of cncx-dimer and AM@cncx Complexes

4.5 IRI Analysis

By employing interaction region indicator (IRI) analysis, we can computationally explore and comprehend the different interactions occurring within and between molecules. This method involves visualizing the overlap of electron density in different regions, utilizing both 3D surfaces and 2D IRI graphs. The interaction region indicator (IRI) allows us to detect covalent and noncovalent interactions equally, and it comes with a lower computational cost [108]. IRI can be expressed as:

$$IRI(r) = \frac{|\nabla\rho\,(\mathrm{r})|}{[\rho\,(\mathrm{r})]^{a}} \qquad (8)$$

Where α =1.1. IRI. sign$(\lambda_2)\rho$ =second largest eigenvalue of Hessian of ρ gives the information about the different types of interactions.

Areas with relatively high ρ, signifying a strong interaction. On the contrary, regions with low ρ, suggesting a weak or negligible interaction, will have a small sign $(\lambda_2)\rho$, possibly due to a very weak interatomic (vdW) interaction.

The nature of interactions shown on IRI isosurfaces can be easily identified by examining the colors mapped from sign$(\lambda_2)\rho$, as illustrated below in **Figure 4.4.**:

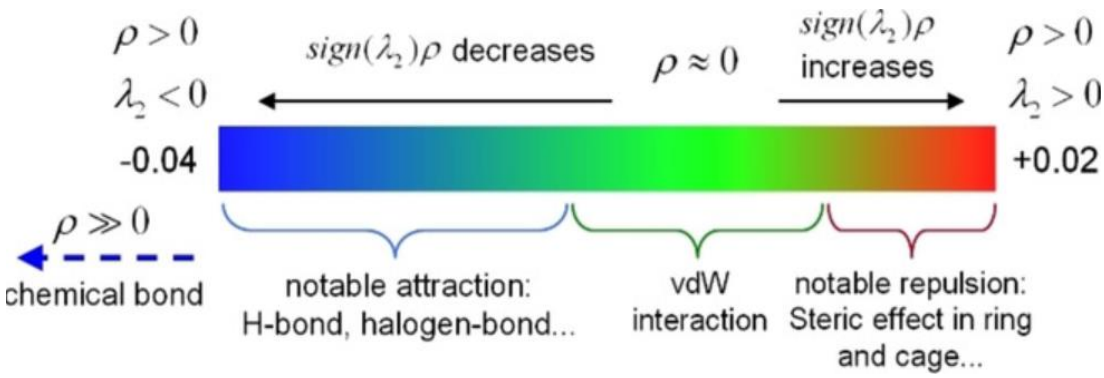

Figure 4.4: Coloring scheme of sign(λ_2)ρ on IRI isosurfaces isosurfaces

The analysis of 3D shapes and 2D maps give insights into the covalent and non-covalent interactions present in AM@cncx complexes. Usually, 3D isosurfaces display different

colors like blue, green, and red, representing noncovalent, attractive, and repulsive interactions. IRI maps with spikes at sign$(\lambda_2)\ \rho$ less than 0 indicates repulsive forces, whereas those with sign$(\lambda_2)\ \rho$ greater than 0 point to weak forces known as dispersive.

The interactions between alkali metals and concave-convex dimer were explored through the generation of isosurfaces and IRI graphs. In the graphs of AM@cncx complexes, green patches signify weak dispersive forces, like van der Waals interactions. The spikes observed around the $(\lambda_2)\ \rho$ region (approximately −0.04 and 0.005 au) denotes week van der Waals interactions (refer to **Figure 4.5**).

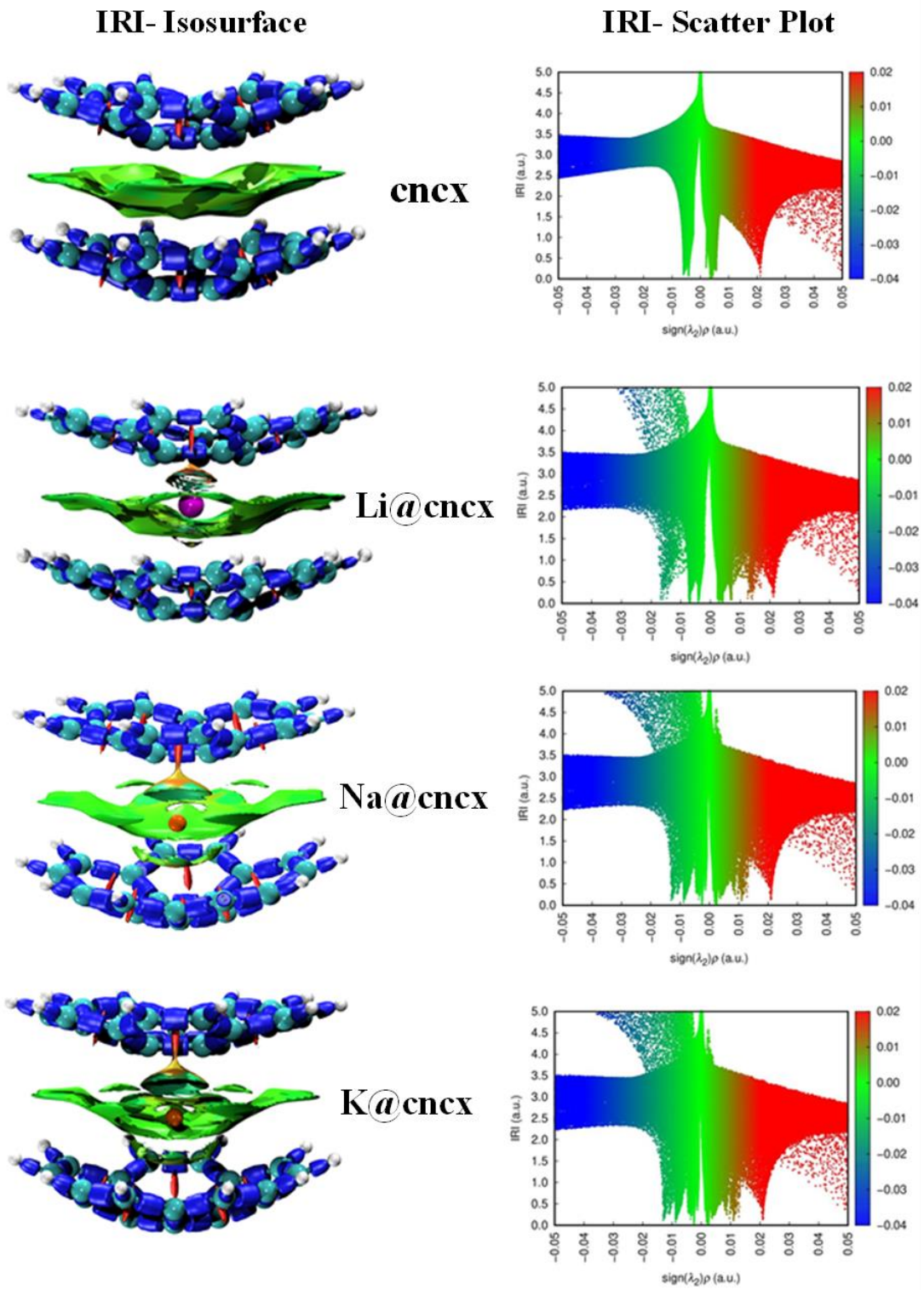

Figure 4.5: 3D Isosurfaces and 2D- graphs of cncx-dimer and AM@cncx Complexes

4.4 Density of states (DOS) analysis

Location of newly created HOMO and the contributions of each fragment in creating these new HOMO, TDOS and PDOS analyses were carried out. To deepen our comprehension of doped complexes, we conducted a density of states analysis, focusing on frontier molecular orbitals (FMO), electronic properties, and energy changes. In the DOS spectra, dotted line representing the newly formed HOMO. The PDOS spectra clearly indicate that dimer plays a significant role in generating new HOMOs. In the AM@cncx dimer, the main contribution comes from the cncx dimer. The newly formed HOMOs in all complexes have higher energy levels, lies between -4 and -5 *eV*, unlike the -8.0 *eV* energy of the HOMO of dimer. The PDOS and TDOS spectra for dimer and the AM@cncx materials are shown in **Figure 4.6**. It is predicted that the introduction of these new HOMOs will play a part in lowering the Eg and enhancing the nonlinear properties.

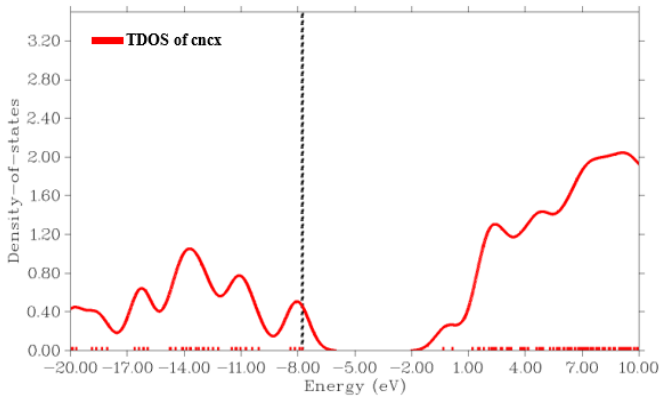

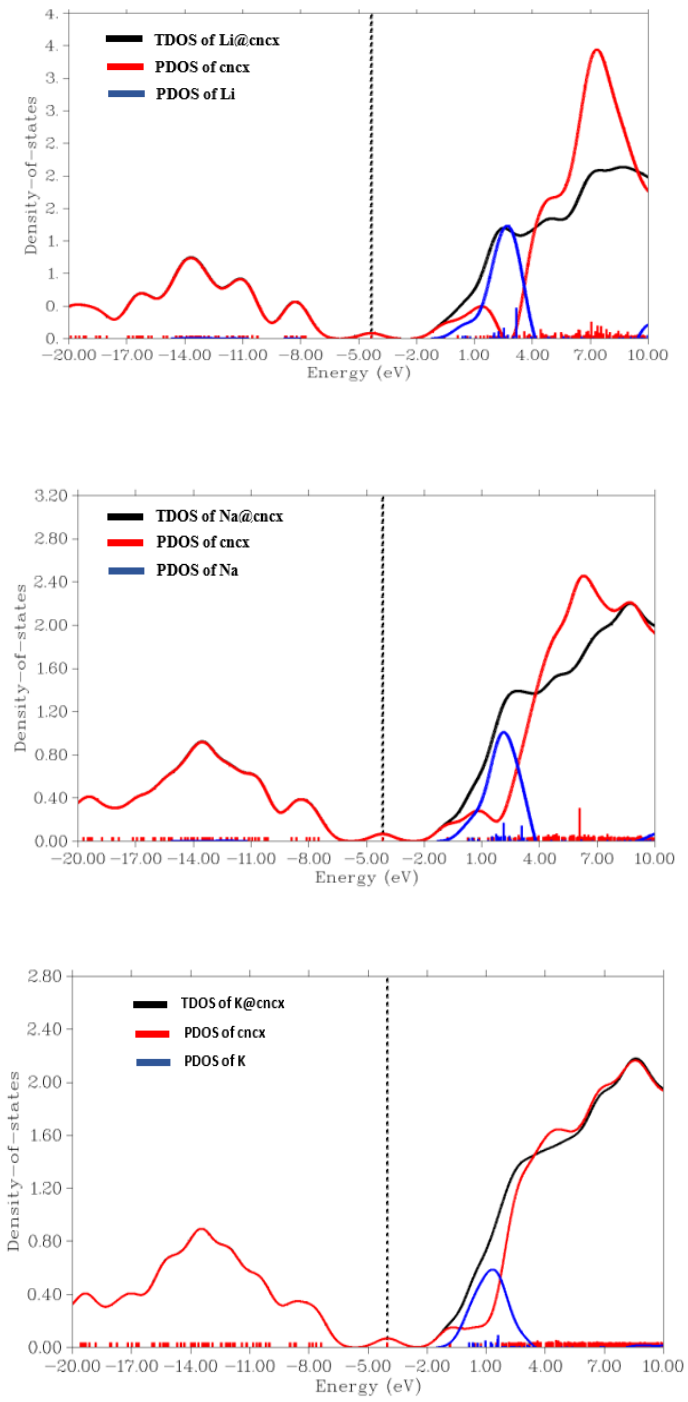

Figure 4.6: Plots of density of state (DOS) of cncx-dimer and AM@cncx

4.5 Molecular Electrostatic Potential (MEP)

MEP is useful for predicting hydrogen bonding interactions and used to indicate the regions that act as nucleophilic and electrophilic [109]. Its indirect involvement is noted in various studies that explore the relationships between structure and properties.

MEP analysis of dimer and alkali metal doped complexes reveals negative (red coded) and positive (blue coded) regions, as depicted in **Figure 4.7**. The dimer exhibits distinct electrophilic and nucleophilic sites. The colour gradient, using blue, and green, illustrates negative, and positive potential regions, respectively. The MEP of dimer represents the negative charge on the concave side and a positive charge on the convex face. In alkali metal-doped complexes, the green region on the concave side indicates an electron-deficient region resulting from electron transfer during complex formation.

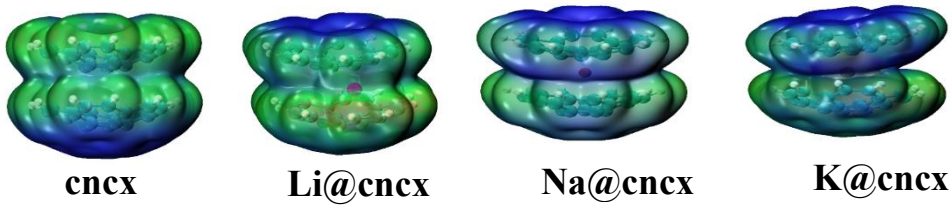

Figure 4.7: Molecular electrostatic potential plots for cncx-dimer and AM@cncx complexes

4.6 Time-Dependent Density Functional (TD-DFT) Calculations

TD-DFT was carried out to know about transparency and potential use of designed complexes. The properties of electronically excited states (ES), transparency of the designed complexes and energies of complexes can be assessed through this approach. TD-DFT analysis revealed the absorption properties of complexes.

Table 4-4: Absorption wavelength, Excitation energy *and oscillator strength* of cncx-dimer and AM@cncx complexes

Complexes	***ΔE* (*eV*)**	***f_o***	***λmax* (*nm*)**	**Major contribution**
cncx	5.70	0.78	217.18	HOMO-2→LUMO+6
Li@cncx	2.18	0.07	568.18	HOMO→LUMO+8
Na@cncx	2.16	0.08	573.71	HOMO→LUMO+9
K@cncx	2.15	0.04	576.26	HOMO→ LUMO+2

Absorption analysis provided a comprehensive examination of the absorption region in the AM@cncx complexes. The absorption region range is 217-576 *nm*, so the designed complexes are UV transparent.

The absorption maxima *(λ_{max})* of AM@cncx complexes exceed the maximum absorption of pure cncx. The absorption spectra of each AM@cncx complex demonstrates a shift toward longer wavelengths in comparison to the pure cncx dimer. All the metal doped complexes absorb in the visible range. Significant transitions are noted at 568, 573, and 576 *nm* with corresponding oscillator strengths *(f_o)* of 0.076, 0.081, and 0.048 for Li@cncx, Na@cncx and K@cncx respectively. For K@cncx λ_{max} of 576.26 *nm* is observed with the lowest excitation energy*(ΔE)*, of 2.15 *eV*. Absorption wavelength shows the designed complexes are considered as UV transparent [110]. UV-VIS spectrum of all complexes (AM@cncx) are presented in **Figure 4.8.**

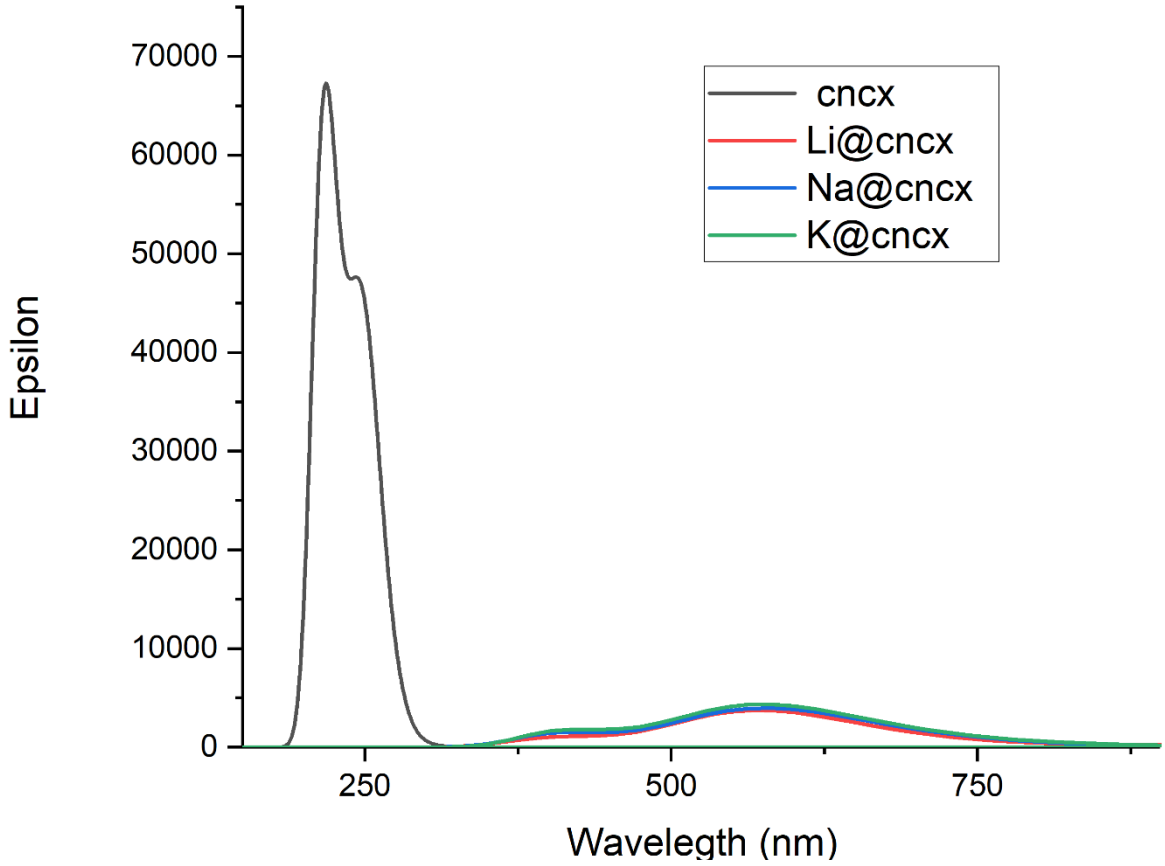

Figure 4.8: UV−Vis spectra of undoped cncx-dimer and AM@cncx

4.7 Nonlinear optical analysis

The excess electrons from alkali metals contribute to enhanced polarization, more charge transfer, leading to the rise in the dipole moment, as well as nonlinear optical characteristics of the AM@cncx complexes. The dipole moment of cncx-dimer is 4.65 *D*.

The dipole moments of complexes range from 3.08 *D* to 5.79 *D*. Among them, the Na@cncx complex exhibits the highest dipole moment at 7.88 *D*, while the lowest dipole moment (3.08 *D*) was observed in Li@cncx as detailed in **Table 4.5**.

Table 4-5: *Δμ (D), α_o (a.u), β_o (a.u)* and β_{Vec} of cncx-dimer and AM@cncx complexes

Complexes	***Δμ (D)***	***α_o (a.u)***	***β_o (a.u)***	***β_{Vec} (a.u)***
cncx	4.65	407	2.9×10^2	4.9×10^2
Li@cncx	3.09	460	9.3×10^4	2.3×10^4
Na@cncx	7.89	457	5.3×10^4	2.1×10^4
K@cncx	5.79	476	3.0×10^4	6.9×10^4

The dimer shows the polarizability up to 407 *au* whereas the range for metal doped complexes is 460 *au* to 476 *au.* This observation is consistent with findings in previous literature, supporting the idea that alkali metal doped dimer exhibit an enhanced nonlinear response [111].

$C_{20}H_{10}$ has (β_0) equal to 74 *au*. Li-$C_{20}H_{10}$ exhibits a β_0 value of 4547 *au*. when lithium is doped on the convex side of corannulene, and 501 *au* when the metal is doped on the concave side of corannulene. Introducing alkali atoms into the cncx dimer has a notable

impact, greatly enhancing the system's α and β. The compound's curved structure leads to significant dipole moments, contributing to heightened π–π intermolecular interactions [112].

The experimental and theoretical evaluation of β_0 is done by analyzing Hyper-Rayleigh scattering (HRS) [113, 114]. β_{HRS} lies in the range from 2.1×10^2 to 4.8×10^4 *au* as outlined in **Table 4.6**. The highest first hyperpolarizability value for Li@cncx complex was compared with other nonlinear optical (NLO) molecules that have a similar magnitude of hyperpolarizability. Our findings reveal that the Li@cncx complex, possess first hyperpolarizability of 9.3 × 104 au, It becomes evident that the highest first hyperpolarizability within the studied complexes, measuring 9.3 × 104 au, is comparable to the previously reported values of 2.31 × 104 au, 2.85 × 103 au, and 3.09 × 103 au for lithium-doped decaborane (Li@B10H14) and halide ion complexes of decaboranes (I−@B10H14 & I−@2,4-I2B10H12) [19]. Alkali metal doped complexes with significant βo values are considered more attractive as NLO candidates.

In addition to examining static hyperpolarizability, simulations were conducted to explore the dynamic hyperpolarizability *(β (ω))*, of the designed complexes. These simulations were performed at standard laser wavelengths 1034 *nm*, 1550 *nm*, and 1907 *nm*. EOPE (electro-optical Pockel's effect) and SHG (second harmonic generation) were calculated. For all AM@cncx complexes, the values of EOPE β *(−ω, ω,0)* and SHG β *(-2ω; ω, ω)* was increased..

Table 4-6: Frequency dependent hyperpolarizability values for of cncx-dimer and AM@cncx complexes at different wavelengths (λ values in nm and all other values in au)

Complexes	**EOPE *(-ω, ω, 0)***			**SHG *(-2ω, ω, ω)***			**HRS *(-2ω, ω, ω)***		
	λ=1907	λ=1550	λ=1340	λ=1907	λ=1550	λ=1340	λ=1907	λ=1550	λ=1340

cncx	3.0×10^{2}	3.0×10^{2}	3.1×10^{2}	3.2×10^{2}	3.3×10^{2}	3.4×10^{2}	2.2×10^{2}	2.2×10^{2}	2.3×10^{2}
Li@cncx	1.8×10^{5}	4.6×10^{5}	2.7×10^{4}	3.4×10^{4}	2.9×10^{4}	5.3×10^{3}	4.8×10^{4}	1.2×10^{5}	1.0×10^{4}
Na@cncx	5.2×10^{5}	1.0×10^{4}	1.3×10^{3}	2.8×10^{4}	1.5×10^{3}	2.4×10^{3}	2.9×10^{4}	4.1×10^{3}	3.7×10^{3}
K@cncx	1.7×10^{5}	7.3×10^{3}	8.9×10^{2}	1.9×10^{4}	3.6×10^{3}	7.0×10^{3}	2.0×10^{4}	5.0×10^{3}	4.8×10^{3}

Frequency dependent hyperpolarizability values, including EOPE *(-ω, ω, 0)* and SHG*(-2ω, ω, ω)*), at three laser wavelengths 1340 *nm*, 1550 *nm*, and 1064 *nm*. The EOPE values, reaching substantial magnitudes, extend from 8.9×10^{2} *au* to 4.6×10^{5} *au* across all mentioned wavelengths. Likewise, SHG values exhibit an increase, ranging from 3.6×10^{3} *au* to 3.4×10^{4} *au* at all mentioned wavelengths, as outlined in **Table 4.7**

Table 4-7: EOKE & EFISHG coefficients *(au)*, γ^{DFWM} and nonlinear refractive indices ($cm^2\ W^{-1}$)

Complexes	**Wavelength (nm)**	***γ (-ω; ω,0,0)* EOKE**	***γ (-2ω; ω,ω,0)* EFISHG**	γ^{DFWM} ***(-ω;ω,-ω,ω)***	n_2 ($cm^2\ W^{-1}$)
cncx	1907	1.1×10^{5}	1.1×10^{5}	1.2×10^{5}	9.4×10^{-18}
	1550	1.1×10^{5}	1.2×10^{5}	1.1×10^{5}	6.0×10^{-13}
	1340	1.1×10^{5}	1.2×10^{5}	1.1×10^{5}	9.9×10^{-18}
Li@cncx	1907	4.5×10^{8}	3.3×10^{7}	4.5×10^{8}	3.8×10^{-14}
	1550	7.3×10^{8}	6.9×10^{7}	7.3×10^{9}	6.6×10^{-13}
	1340	4.8×10^{7}	4.2×10^{6}	1.4×10^{6}	1.0×10^{-16}
Na@cncx	1907	1.0×10^{10}	3.6×10^{7}	1.0×10^{10}	8.2×10^{-13}
	1550	1.2×10^{7}	1.1×10^{6}	6.8×10^{3}	5.6×10^{-19}
	1340	3.3×10^{6}	7.9×10^{4}	4.3×10^{4}	3.5×10^{-18}

K@cncx	1907	2.9×10^{9}	6.1×10^{7}	2.9×10^{9}	2.4×10^{-13}
	1550	7.3×10^{3}	3.6×10^{3}	2.6×10^{6}	2.1×10^{-16}
	1340	3.3×10^{6}	7.9×10^{4}	2.2×10^{6}	1.8×10^{-16}

Considering all the studied metal-doped complexes, the values of the estimated electro-optic Kerr's effect($\gamma(-\omega;\ \omega,0,0)$ EOKE) varied between 1.1×10^{5} to 4.8×10^{7} *au* at 1340 nm, the range is 7.3×10^{3} to 7.3×10^{8} at 1550 nm, and at 1907 nm from 1.1×10^{5} to 1.0×10^{10} *au*. For all the studied alkali metal-doped complexes, the Electric-field-induced second-harmonic generation ($\gamma(-2\omega;\ \omega,\ \omega,\ 0)$ EFISHG) values were in the range of 7.9×10^{4} to 4.2×10^{6} *au* at 1340 *nm*, from 1.1×10^{5} to 6.9×10^{7} *au* at 1550 *nm*, and from 1.1×10^{5} to 6.9×10^{7} *au* at 1907 *nm*. It is evident from the results (**Table 4.7**) that Li@cncx complex has the maximum value of EFISHG (6.9×10^{7} *au*) at 1550 *nm* and Na@cncx has maximum EOKE (1.0×10^{10} *au*) coefficients at 1907 *nm*.

Additionally, the calculation of quadratic nonlinear refractive indices (n_2) for all designed NLO complexes have been conducted [115]. the quadratic nonlinear refractive index values was computed to know the potential applications of the designed complexes [116].

$$n2\left(\frac{cm^2}{W}\right) = 8.28 \text{ x } 10^{-23}\gamma DFWM$$

The quadratic nonlinear refractive indices were increased for all the AM@cncx complexes, as detailed in **Table 4.7** Its value vary with different wavelength, the value range for cncx is (6.0×10^{-13} *au* to 9.9×10^{-18} *au*), for Li@cncx (6.6×10^{-13} *au* to 1.0×10^{-16} *au*), for Na@cncx(5.6×10^{-19} *au*-8.2×10^{-13} *)*. The study observes a significant increase in nonlinear optical response with wavelength variation, especially in the nonlinear refractive index for all designed complexes.

Chapter 5
Conclusion

In this work, the geometrical, electrical, and nonlinear optical (NLO) properties of dimer, especially when doped with alkali metals, were analyzed by DFT. The results show that doping with alkali metals significantly improves the dimer's NLO response. The interaction energies computed computationally, which range from -22.2 to -34.5 *eV*, confirm that the newly developed alkali metal-doped dimers are stable. Significant charge transfer from alkali metals to the cncx dimer is revealed by NBO analysis, with the K@cncx complex showing the largest charge transfer.

Moreover, doping the complexes with metal atoms significantly lowers their HOMO-LUMO energy gap by as much as 3.17 *eV*. The participation of metal and dimer in the creation of new HOMO states in the presence of excess electrons is confirmed by the PDOS spectra of doped complexes. The alkali metal-doped complexes show significantly larger static hyperpolarizabilities *(β0)* than the undoped dimer in the 3.0×10^4–9.3×10^4 *au* range. Li@cncx is unique among these complexes, having the highest thermodynamic stability and the highest hyperpolarizability value of 9.3×10^4 *au*. The study also determines frequency-dependent Second Harmonic Generation (SHG), Electric-Optical Pockels Effect (EOPE), electro-optic dc-Kerr effect (EOKE). The value of 3.4×10^4 *au* is observed for SHG, while for EOPE the value is 4.6×10^5 *au*. A significantly enhanced EOKE value (1.0×10^{10} *au*) is shown by Na@cncx. Additionally, these structures exhibit a high nonlinear quadratic refractive index (a maximum value of $9.9\times10^{-18} cm^2\ W^{-1}$). The study concludes by predicting that NLO materials with exceptional performance and outstanding NLO response will be produced by alkali metal dopants.

References

1. Suresh, S., et al., *Review on theoretical aspect of nonlinear optics.* Rev. Adv. Mater. Sci, 2012. **30**(2): p. 175-183.

2. Oudar, J.t. and R. Hierle, *An efficient organic crystal for nonlinear optics: methyl-(2, 4-dinitrophenyl)-aminopropanoate.* Journal of applied physics, 1977. **48**(7): p. 2699-2704.

3. Marder, S.R., J.E. Sohn, and G.D. Stucky, *Materials for nonlinear optics: chemical perspectives*. 1991: ACS Publications.

4. Etter, M.C., *Encoding and decoding hydrogen-bond patterns of organic compounds.* Accounts of Chemical Research, 1990. **23**(4): p. 120-126.

5. Nalwa, H.S., *Organometallic materials for nonlinear optics.* Applied organometallic chemistry, 1991. **5**(5): p. 349-377.

6. Berthier, G., et al., *Dipole moments and polarizabilities of some substituted pyridine-1-oxides for optoelectronics.* Journal of Molecular Structure: THEOCHEM, 1992. **254**: p. 205-218.

7. Zyss, J. and I. Ledoux, *Nonlinear optics in multipolar media: theory and experiments.* Chemical reviews, 1994. **94**(1): p. 77-105.

8. Vijayakumar, T., et al., *Efficient π electrons delocalization in prospective push–pull non-linear optical chromophore 4-[N, N-dimethylamino]-4'-nitro stilbene (DANS): A vibrational spectroscopic study.* Chemical Physics, 2008. **343**(1): p. 83-99.

9. Van Cleuvenbergen, S., et al., *ZIF-8 as nonlinear optical material: influence of structure and synthesis.* Chemistry of Materials, 2016. **28**(9): p. 3203-3209.

10. Nakano, M., et al., *Spin multiplicity effects on the second hyperpolarizability of an open-shell neutral π-conjugated system.* The Journal of Physical Chemistry A, 2004. **108**(18): p. 4105-4111.

11. Nakano, M., et al., *Second hyperpolarizabilities (γ) of bisimidazole and bistriazole benzenes: diradical character, charged state, and spin state dependences.* The Journal of Physical Chemistry A, 2006. **110**(12): p. 4238-4243.

12. Nakano, M., et al., *Relationship between third-order nonlinear optical properties and magnetic interactions in open-shell systems: a new paradigm for nonlinear optics.* Physical review letters, 2007. **99**(3): p. 033001.

13. Qiu, Y.-Q., et al., *Theoretical Study on the Relationship between Spin Multiplicity Effects and Nonlinear Optical Properties of the Pyrrole Radical (C4H4N⊙).* The Journal of Physical Chemistry A, 2008. **112**(1): p. 83-88.

14. Li, Y., et al., *An ab initio prediction of the extraordinary static first hyperpolarizability for the electron-solvated cluster (FH) 2 {e}(HF).* The Journal of Physical Chemistry B, 2004. **108**(10): p. 3145-3148.

15. Hou, N., Y. Wu, and H. Wu, *The Influence of Alkali metals Interaction with Al/P-Substituted BN Nanosheets on Their Electronic and Nonlinear Optical Properties: A DFT Theoretical Study.* ChemistrySelect, 2019. **4**(4): p. 1441-1447.

16. Rashid, M., et al., *Nonlinear optical (NLO) response of boron phosphide nanosheet by alkali metals doping: A DFT study.* Materials Science in Semiconductor Processing, 2022. **151**: p. 107007.

17. Chen, W., et al., *Nonlinear optical properties of alkalides Li+ (calix [4] pyrrole) M-(M= Li, Na, and K): alkali anion atomic number dependence.* Journal of the American Chemical Society, 2006. **128**(4): p. 1072-1073.

18. Xu, H.-L., et al., *Lithiation and Li-doped effects of [5] cyclacene on the static first hyperpolarizability.* The Journal of Physical Chemistry C, 2009. **113**(12): p. 4984-4986.

19. Muhammad, S., et al., *Quantum mechanical design and structure of the Li@ B10H14 basket with a remarkably enhanced electro-optical response.* Journal of the American Chemical Society, 2009. **131**(33): p. 11833-11840.

20. Liu, S., et al., *Transition metals doped fullerenes: structures–NLO property relationships.* Molecular Physics, 2019. **117**(6): p. 705-711.

21. Li, Z.-J., et al., *A dependence on the petal number of the static and dynamic first hyperpolarizability for electride molecules: many-petal-shaped Li-doped cyclic polyamines.* The Journal of Physical Chemistry A, 2009. **113**(12): p. 2961-2966.

22. Shakerzadeh, E., Z. Biglari, and E. Tahmasebi, *M@ B40 (M= Li, Na, K) serving as a potential promising novel NLO nanomaterial.* Chemical Physics Letters, 2016. **654**: p. 76-80.

23. Xu, H.-L., et al., *Structures and large NLO responses of new electrides: Li-doped fluorocarbon chain.* Journal of the American Chemical Society, 2007. **129**(10): p. 2967-2970.

24. Rahman, A.U., et al., *Tunable electronic and magnetic properties of single layer CdS via Li substitutional doping: A first-principle study.* Journal of Physics and Chemistry of Solids, 2022. **161**: p. 110380.

25. Ahsan, A., et al., *Endohedral metallofullerene electrides of Ca 12 O 12 with remarkable nonlinear optical response.* RSC advances, 2021. **11**(3): p. 1569-1580.

26. Kosar, N., et al., *Significant nonlinear optical response of alkaline earth metals doped beryllium and magnesium oxide nanocages.* Materials Chemistry and Physics, 2020. **242**: p. 122507.

27. Chen, C., et al., *A new-type ultraviolet SHG crystal-beta-BaB2O4.* Scientia Sinica Series B-Chemical Biological Agricultural Medical & Earth Sciences, 1985. **28**(3): p. 235-243.

28. Chen, C., et al., *New nonlinear-optical crystal: LiB 3 O 5.* JOSA B, 1989. **6**(4): p. 616-621.

29. HAUSSÜHL, S., *Elastische und thermoelastische eigenschaften von KH2PO4, KH2AsO4, NH4H2PO4, NH4H2AsO4 und RbH2PO4.* Zeitschrift für Kristallographie-Crystalline Materials, 1964. **120**(1-6): p. 401-414.

30. Bierlein, J.D. and H. Vanherzeele, *Potassium titanyl phosphate: properties and new applications.* JOSA B, 1989. **6**(4): p. 622-633.

31. Li, Y.-Y., et al., *Mixed-anion inorganic compounds: a favorable candidate for infrared nonlinear optical materials.* Crystal Growth & Design, 2019. **19**(7): p. 4172-4192.

32. Bouchouit, K., et al., *Reversible phase transition in semi-organic compound p-Nitroanilinium sulfate detected using second harmonic generation as a tool.* Optical Materials, 2015. **48**: p. 215-221.

33. Kroto, H.W., et al., *C60: Buckminsterfullerene.* nature, 1985. **318**(6042): p. 162-163.

34. Haymet, A.D., *C120 and C60: Archimedean solids constructed from sp2 hybridized carbon atoms.* Chemical physics letters, 1985. **122**(5): p. 421-424.

35. Haddon, R., L.E. Brus, and K. Raghavachari, *Electronic structure and bonding in icosahedral C60.* Chemical Physics Letters, 1986. **125**(5-6): p. 459-464.

36. Liu, Q., et al., *The applications of buckminsterfullerene C60 and derivatives in orthopaedic research.* Connective tissue research, 2014. **55**(2): p. 71-79.

37. Senftleben, O., et al., *C60 nanostructures for applications in information technology.* Advanced Engineering Materials, 2009. **11**(4): p. 278-284.

38. Tutt, L.W. and A. Kost, *Optical limiting performance of C60 and C70 solutions.* Nature, 1992. **356**(6366): p. 225-226.

39. Delgado, J.L., et al., *Buckyballs.* Polyarenes II, 2014: p. 1-64.

40. Hawkins, J.M., et al., *Crystal structure of osmylated C60: confirmation of the soccer ball framework.* Science, 1991. **252**(5003): p. 312-313.

41. Kang, J., et al., *C 5-Symmetric chiral corannulenes: desymmetrization of bowl inversion equilibrium via "intramolecular" hydrogen-bonding network.* Journal of the American Chemical Society, 2014. **136**(30): p. 10640-10644.

42. Zoppi, L., L. Martin-Samos, and K.K. Baldridge, *Effect of molecular packing on corannulene-based materials electroluminescence.* Journal of the American Chemical Society, 2011. **133**(35): p. 14002-14009.

43. Stöckl, Q., et al., *Gear-meshed tiling of surfaces with molecular pentagonal stars.* Journal of the American Chemical Society, 2014. **136**(2): p. 606-609.

44. Bauert, T., et al., *Large induced interface dipole moments without charge transfer: Buckybowls on metal surfaces.* The Journal of Physical Chemistry Letters, 2011. **2**(21): p. 2805-2809.

45. Bauert, T., et al., *Quadruple anionic buckybowls by solid-state chemistry of corannulene and cesium.* Journal of the American Chemical Society, 2013. **135**(34): p. 12857-12860.

46. Zhang, Q., et al., *Palladium-catalyzed C–H activation taken to the limit. Flattening an aromatic bowl by total arylation.* Journal of the American Chemical Society, 2012. **134**(38): p. 15664-15667.

47. Schmidt, B.M. and D. Lentz, *Syntheses and properties of buckybowls bearing electron-withdrawing groups.* Chemistry Letters, 2014. **43**(2): p. 171-177.

48. Utko, P., et al., *Sub-Kelvin transport spectroscopy of fullerene peapod quantum dots.* Applied physics letters, 2006. **89**(23).

49. Sato, S., T. Yamasaki, and H. Isobe, *Solid-state structures of peapod bearings composed of finite single-wall carbon nanotube and fullerene molecules.* Proceedings of the National Academy of Sciences, 2014. **111**(23): p. 8374-8379.

50. Sygula, A., et al., *'Buckybowls'—introducing curvature by solution phase synthesis.* Tetrahedron, 2001. **57**(17): p. 3637-3644.

51. Barth, W.E. and R.G. Lawton, *Dibenzo [ghi, mno] fluoranthene.* Journal of the American Chemical Society, 1966. **88**(2): p. 380-381.

52. Hanson, J.C. and C. Nordman, *The crystal and molecular structure of corannulene, C20H10.* Acta Crystallographica Section B: Structural Crystallography and Crystal Chemistry, 1976. **32**(4): p. 1147-1153.

53. Scott, L.T., *Fragments of fullerenes: novel syntheses, structures and reactions.* Pure and applied chemistry, 1996. **68**(2): p. 291-300.

54. Tsefrikas, V.M. and L.T. Scott, *Geodesic polyarenes by flash vacuum pyrolysis.* Chemical reviews, 2006. **106**(12): p. 4868-4884.

55. Wu, Y.-T. and J.S. Siegel, *Aromatic molecular-bowl hydrocarbons: synthetic derivatives, their structures, and physical properties.* Chemical reviews, 2006. **106**(12): p. 4843-4867.

56. Sygula, A., *Chemistry on a Half-Shell: Synthesis and Derivatization of Buckybowls.* European Journal of Organic Chemistry, 2011. **2011**(9): p. 1611-1625.

57. Wu, Y.-T. and J.S. Siegel, *Synthesis, structures, and physical properties of aromatic molecular-bowl hydrocarbons.* Polyarenes I, 2014: p. 63-120.

58. Sygula, A., *Corannulene-adorned molecular receptors for fullerenes utilizing the π–π stacking of curved-surface conjugated carbon networks. design, synthesis and testing.* Synlett, 2016. **27**(14): p. 2070-2080.

59. Saito, M., H. Shinokubo, and H. Sakurai, *Figuration of bowl-shaped π-conjugated molecules: properties and functions.* Materials Chemistry Frontiers, 2018. **2**(4): p. 635-661.

60. Zabula, A.V., et al., *Record alkali metal intercalation by highly charged corannulene.* Accounts of Chemical Research, 2018. **51**(6): p. 1541-1549.

61. Nestoros, E. and M.C. Stuparu, *Corannulene: a molecular bowl of carbon with multifaceted properties and diverse applications.* Chemical Communications, 2018. **54**(50): p. 6503-6519.

62. Haupt, A. and D. Lentz, *Corannulenes with Electron-Withdrawing Substituents: Synthetic Approaches and Resulting Structural and Electronic Properties.* Chemistry–A European Journal, 2019. **25**(14): p. 3440-3454.

63. Muzammil, E.M., D. Halilovic, and M.C. Stuparu, *Synthesis of corannulene-based nanographenes.* Communications Chemistry, 2019. **2**(1): p. 58.

64. Barát, V. and M.C. Stuparu, *Corannulene Chalcogenides.* Chemistry–An Asian Journal, 2021. **16**(1): p. 20-29.

65. Li, X., F. Kang, and M. Inagaki, *Buckybowls: Corannulene and its derivatives.* Small, 2016. **12**(24): p. 3206-3223.

66. Grabowsky, S., et al., *Electron density of corannulene from synchrotron data at 12 K, comparison with fullerenes.* Zeitschrift für Naturforschung B, 2010. **65**(4): p. 452-460.

67. Palacin, S., et al., *Hydrogen-bonded tapes based on symmetrically substituted diketopiperazines: a robust structural motif for the engineering of molecular solids.* Journal of the American Chemical Society, 1997. **119**(49): p. 11807-11816.

68. Han, X., et al., *Aggregation-induced emission materials for nonlinear optics.* Aggregate, 2021. **2**(3): p. e28.

69. Janowski, T., et al., *Convex–concave stacking of curved conjugated networks: Benchmark calculations on the corannulene dimer.* Chemical Physics Letters, 2011. **512**(4-6): p. 155-160.

70. Sanyal, S., A.K. Manna, and S.K. Pati, *Functional corannulene: diverse structures, enhanced charge transport, and tunable optoelectronic properties.* ChemPhysChem, 2014. **15**(5): p. 885-893.

71. Wu, Y.-L., et al., *Structural, optical, and electrochemical properties of three-dimensional push–pull corannulenes.* The Journal of Organic Chemistry, 2012. **77**(24): p. 11014-11026.

72. Zoppi, L., A. Ferretti, and K.K. Baldridge, *Static and field-oriented properties of bowl-shaped polynuclear aromatic hydrocarbon fragments.* Journal of Chemical Theory and Computation, 2013. **9**(11): p. 4797-4804.

73. Becker, H., et al., *Gas-phase ion/molecule reactions of corannulene, a fullerene subunit.* Journal of the American Chemical Society, 1993. **115**(24): p. 11636-11637.

74. Wong, B.M., *Noncovalent interactions in supramolecular complexes: A study on corannulene and the double concave buckycatcher.* Journal of computational chemistry, 2009. **30**(1): p. 51-56.

75. Franken, e.P., et al., *Generation of optical harmonics.* Physical review letters, 1961. **7**(4): p. 118.

76. Terhune, R., P. Maker, and C. Savage, *Optical harmonic generation in calcite.* Physical Review Letters, 1962. **8**(10): p. 404.

77. Ayalon, A., et al., *Stable high-order molecular sandwiches: hydrocarbon polyanion pairs with multiple lithium ions inside and out.* Science, 1994. **265**(5175): p. 1065-1067.

78. Shamlouei, H.R. and F. Parvinzadeh, *Influence of alkali metal atoms on structure, electronic and non-linear optical properties of calix [4] arene.* Physica E: Low-dimensional Systems and Nanostructures, 2021. **127**: p. 114539.

79. Imamura, K., et al., *Triphenyleno [1, 12-bcd: 4, 5-b' c' d': 8, 9-b "c "d "] trithiophene: the first bowl-shaped heteroaromatic.* Chemical Communications, 1999(18): p. 1859-1860.

80. Mizyed, S., et al., *Embracing C60 with multiarmed geodesic partners.* Journal of the American Chemical Society, 2001. **123**(51): p. 12770-12774.

81. Klapwijk, T. *Physics of tunneling barriers*. in *SQUID'85 Superconducting Quantum Interference Devices and their Applications: Proceedings of the Third International Conference on Superconducting Quantum Devices, Berlin (West), June 25-28, 1985*. 2012. Walter de Gruyter.

82. Sohail, M., et al., *Influence of bi-alkali metals doping over Al12N12 nanocage on stability and optoelectronic properties: A DFT investigation.* Radiation Physics and Chemistry, 2021. **184**: p. 109457.

83. Tolbin, A.Y., et al., *Peripheral functionalisation of a stable phthalocyanine J-type dimer to control the aggregation behaviour and NLO properties: UV-Vis, fluorescence, DFT, TDHF and thermal study.* RSC advances, 2015. **5**(11): p. 8239-8247.

84. Kato, K., et al., *Synthesis, Properties, and Packing Structures of Corannulene-Based π-Systems Containing Heptagons.* Chemistry–An Asian Journal, 2015. **10**(8): p. 1635-1639.

85. Liu, Y.M., et al., *Functional Sulfur-Doped Buckybowls and Their Concave–Convex Supramolecular Assembly with Fullerenes.* Angewandte Chemie International Edition, 2016. **55**(42): p. 13047-13051.

86. Scott, L.T., *Methods for the chemical synthesis of fullerenes.* Angewandte Chemie International Edition, 2004. **43**(38): p. 4994-5007.

87. Iqbal, J., R. Ludwig, and K. Ayub, *Phosphides or nitrides for better NLO properties? A detailed comparative study of alkali metal doped nano-cages.* Materials Research Bulletin, 2017. **92**: p. 113-122.

88. Li, X., et al., *Effect of alkali metal atoms doping on structural and nonlinear optical properties of the gold-germanium bimetallic clusters.* Nanomaterials, 2017. **7**(7): p. 184.

89. Munsif, S., et al., *Remarkable nonlinear optical response of alkali metal doped aluminum phosphide and boron phosphide nanoclusters.* Journal of Molecular Liquids, 2018. **271**: p. 51-64.

90. Li, X. and S. Li, *Investigations of electronic and nonlinear optical properties of single alkali metal adsorbed graphene, graphyne and graphdiyne systems by first-principles calculations.* Journal of Materials Chemistry C, 2019. **7**(6): p. 1630-1640.

91. Chen, C., *Advanced Nonlinear Optical Microscopy for Structural and Functional Imaging of Living Brain*. 2021: Hong Kong University of Science and Technology (Hong Kong).

92. Peyghan, A.A. and M. Noei, *The alkali and alkaline earth metal doped ZnO nanotubes: DFT studies.* Physica B: Condensed Matter, 2014. **432**: p. 105-110.

93. Kosar, N., et al., *DFT studies of single and multiple alkali metals doped C24 fullerene for electronics and nonlinear optical applications.* Journal of Molecular Graphics and Modelling, 2021. **105**: p. 107867.

94. Maqsood, N., et al., *DFT study of alkali and alkaline earth metal-doped benzocryptand with remarkable NLO properties.* RSC advances, 2022. **12**(25): p. 16029-16045.

95. Mandal, U., et al., *Single alkali metal-doped hexalithioborazine complexes with exceptionally high value of polarizability and first hyperpolarizability: a DFT-based computational study.* Theoretical Chemistry Accounts, 2023. **142**(12): p. 122.

96. Roy, D., T.A. Keith, and J.M.J.S.I. Millam, Shawnee Mission, *Current version: GaussView, version 6.* 2016.

97. Frisch, M.e., et al., *Gaussian 16, revision C. 01*. 2016, Gaussian, Inc., Wallingford CT.

98. Rad, A.S., K.J.M.C. Ayub, and Physics, *Adsorption properties of acetylene and ethylene molecules onto pristine and nickel-decorated Al12N12 nanoclusters.* 2017. **194**: p. 337-344.

99. Lu, T. and F. Chen, *Multiwfn: a multifunctional wavefunction analyzer.* Journal of computational chemistry, 2012. **33**(5): p. 580-592.

100. Jiang, Y., et al., *DFT study on nonlinear optical properties of lithium-doped corannulene.* Chinese Science Bulletin, 2012. **57**: p. 4448-4452.

101. Sygula, A. and S. Saebø, *π-π Stacking of curved carbon networks: The corannulene dimer.* International Journal of Quantum Chemistry, 2009. **109**(1): p. 65-72.

102. Wang, L., et al., *The shape selectivity of corannulene dimers based on concave–convex and convex–convex shape complementarity as hosts for C 60 and C 70.* Physical Chemistry Chemical Physics, 2021. **23**(1): p. 405-414.

103. Ma, J.C. and D.A. Dougherty, *The cation− π interaction.* Chemical reviews, 1997. **97**(5): p. 1303-1324.

104. Gilani, M.A., et al., *Copper-doped Al 12 N 12 nano-cages: potential candidates for nonlinear optical materials.* Applied Physics A, 2018. **124**: p. 1-9.

105. Bader, R.F., *Atoms in molecules.* Accounts of chemical research, 1985. **18**(1): p. 9-15.

106. Bader, R.F. and H. Essén, *The characterization of atomic interactions.* The Journal of chemical physics, 1984. **80**(5): p. 1943-1960.

107. Kumar, P.S.V., V. Raghavendra, and V. Subramanian, *Bader's theory of atoms in molecules (AIM) and its applications to chemical bonding.* Journal of Chemical Sciences, 2016. **128**: p. 1527-1536.

108. Lu, T. and Q. Chen, *Interaction region indicator: A simple real space function clearly revealing both chemical bonds and weak interactions.* Chemistry-Methods, 2021. **1**(5): p. 231-239.

109. Uzun, S., et al., *Experimental and density functional theory (MEP, FMO, NLO, Fukui functions) and antibacterial activity studies on 2-amino-4-(4-nitrophenyl)-5, 6-dihydrobenzo [h] quinoline-3-carbonitrile.* Journal of Molecular Structure, 2019. **1178**: p. 450-457.

110. Shen, Y., et al., *Deep-ultraviolet transparent Cs2LiPO4 exhibits an unprecedented second harmonic generation.* Chemistry of Materials, 2016. **28**(19): p. 7110-7116.

111. Li, W.-Q., et al., *A nonlinear optical switch induced by conformation conversion of alkali metal doped nano-carbon bowls.* Chemical Physics Letters, 2013. **588**: p. 131-135.

112. Delgado, M.C.R., et al., *Tuning the charge-transport parameters of perylene diimide single crystals via end and/or core functionalization: a density functional theory investigation.* Journal of the American Chemical Society, 2010. **132**(10): p. 3375-3387.

113. Kaatz, P. and D.P. Shelton, *Polarized hyper-Rayleigh light scattering measurements of nonlinear optical chromophores.* The Journal of chemical physics, 1996. **105**(10): p. 3918-3929.

114. Hendrickx, E., K. Clays, and A. Persoons, *Hyper-Rayleigh scattering in isotropic solution.* Accounts of Chemical Research, 1998. **31**(10): p. 675-683.

115. Lu, S., et al., *Third order nonlinear optical property of Bi 2 Se 3.* Optics express, 2013. **21**(2): p. 2072-2082.

116. Bree, C., A. Demircan, and G. Steinmeyer, *Method for computing the nonlinear refractive index via Keldysh theory.* IEEE Journal of Quantum Electronics, 2010. **46**(4): p. 433-437.